TECHNICAL ARTICLE

Cyclic Deformation Behavior and Failure Mechanism of 316LN Stainless Steel under Creep-Fatigue Loading at 550 °C

Jingwei Zhao, Bingbing Li, Yiming Zheng, Mohammad Azadi, and Xu Chen

A comparative study on the low-cycle fatigue properties of 316LN austenitic stainless steel with and without a hold period at the maximum tensile strain was performed. Different hold periods (0 s, 60 s, 120 s, 300 s, 1800 s) at a constant strain amplitude of ±0.8% were employed in creep-fatigue tests at 550 °C. Dynamic strain aging (DSA), creep and thermal recovery dominated the deformation and failure behavior. The evolution process of DSA activity and stress relaxation caused by creep presented an opposite trend during cycling. The amount of stress relaxation increased while the associated inelastic strain rate decreased with increasing dwell time, which promoted the accumulation of intergranular damage per cycle and facilitated the formation of dislocation cells. The enhanced process of cross-slip attenuated the DSA activity, which compensated for the increased creep damage; thus, the fatigue life remained almost constant after the introduction of a hold period of 300 s. Interestingly, the fatigue life showed a slight increase when the hold period increased to 1800 s due to the increased thermal recovery process.

1. Introduction

316LN austenitic stainless steel (SS) is now widely used as the main structural material for piping systems in fourth-generation sodium-cooled fast reactors (SFRs) due to its excellent combination of mechanical properties and corrosion resistance at high temperatures (Ref 1, 2). Pipelines are generally subjected to repeated thermal stress due to the temperature gradient that forms during start-up and shutdown processes and under substantial thermal transient conditions. Accordingly, low-cycle fatigue (LCF) failure has become an important life-limiting factor of SFR nuclear power plants. In addition, during the long-term service of SFRs at a high temperature of ~550 °C, the creep damage caused by mechanical loads, such as internal pressure and dead weight, is significantly enhanced, which accelerates damage accumulation and degrades material performance (Ref 3, 4). More importantly, it has been widely demonstrated that the occurrence of creep-fatigue interactions leads to a more dangerous situation in terms of structural integrity at elevated temperatures than the individual action of fatigue or creep (Ref 2-8).

The creep-fatigue interaction is a complex issue involving the synergistic effects of temperature, strain cycles and various time-dependent processes and is frequently used to simulate real service conditions and establish damage evaluation criteria for structures at high temperatures (Ref 9, 10). Although many studies have been performed on the creep-fatigue behaviors of 304(L) and 316(L) stainless steels (Ref 10-13), much less attention has been given to the creep-fatigue performance of the nitrogen-alloyed 316LN SS. The addition of nitrogen will enhance planar slip and retard DSA, decreasing the hardening magnitude and potentially increasing the fatigue resistance (Ref 6, 9, 14). The limited published studies on the creep-fatigue behavior of 316LN SS have been mainly carried out by scholars in India Gandhi Centre for the Atomic Research, Central Research Institute of Electric Power Industry and Korea Atomic Energy Research Institute due to the wide utilization of 316LN SS in SFRs in India, Japan and Korea (Ref 2, 6, 9, 15). The effects of the strain amplitude, hold period, dwell mode and nitrogen content were reported (Ref 9, 10, 16-18). The tensile hold period is more deleterious than the compressive or symmetrical dwell period (Ref 3, 11, 12, 18, 19); thus, the tensile hold period was employed in this current work. Furthermore, the fracture mode changes from transgranular to intergranular with the introduction of a hold period (Ref 6), and the fatigue life decreases with increasing hold period (Ref 9, 20). In general, the rate of damage accumulation under creep-fatigue interaction conditions is not equivalent to the rate of the linear combination of the damage produced by creep and cyclic mechanical loading alone (Ref 3). The complex mutual interaction of various time-dependent damage mechanisms, including dynamic strain aging (DSA), creep, and oxidation,

Jingwei Zhao, Bingbing Li, and Yiming Zheng, School of Chemical Engineering and Technology, Tianjin University, Tianjin 300350, China; and Tianjin Key Laboratory of Chemical Process Safety and Equipment Technology, Tianjin 300350, China; Mohammad Azadi, Faculty of Mechanical Engineering, Semnan University, Semnan, Iran; Xu Chen, School of Chemical Engineering and Technology, Tianjin University, Tianjin 300350, China; Tianjin Key Laboratory of Chemical Process Safety and Equipment Technology, Tianjin 300350, China; and Zhejiang Institute of Tianjin University, Ningbo 315211, China. Contact e-mail: bingbingli@tju.edu.cn.

accelerates damage accumulation and leads to a shorter fatigue life (Ref 9, 20).

The activated temperature range of DSA is consistent with the servicing temperature regime of SFRs (Ref 21, 22). The phenomenon of DSA is the consequence of the interaction between solute atoms and mobile dislocations during plastic deformation and is influenced by different factors, such as strain rate, temperature and chemical composition, which is manifested by stress serrations in the cyclic stress–strain hysteresis loop (Ref 22-25). DSA enhances the cyclic stress response by hindering the movement of dislocations and promoting planar slip bands, which improves the strength of the material but weakens the material ductility and decreases the fatigue life (Ref 26). As a critical damage mechanism of high-temperature structures fabricated by austenitic stainless steel, creep damage generally occurs at temperatures above $0.4T_m$ (T_m is the melting point in K) (Ref 6, 16), which can produce cavities to soften the material and promote the development of elongated or equiaxed dislocation cells (Ref 3, 16). Creep damage has a deleterious effect on the LCF endurance at elevated temperatures, leading to a transition in terms of the cracking mode from transgranular to intergranular (Ref 13, 17, 18). The mechanism proposed was that the formation of vacancy clusters under an applied tensile stress led to the nucleation of cavities at grain boundaries, which grew rapidly by diffusion and linked together to form intergranular cracks (Ref 11, 13, 27). Thermal recovery becomes significant at temperatures ≥ 823 K in austenitic stainless steel and can promote thermally activated dislocation motion by the cross-slip of screw dislocations and climb of edge dislocations, leading to the annihilation of dislocations (Ref 28). The thermal recovery process is manifested by partial transformation of the interiors of dislocation-dense slip bands into dislocation-free channels, which is enhanced with increasing nitrogen content or decreasing strain rate (Ref 29). Although many studies have dealt with the influence of DSA, creep and recovery on the deformation and failure behavior of stainless steel at high temperatures, the interaction behavior between the three processes and its impact on the creep-fatigue behavior of 316LN SS have been less discussed and are far from clear.

In this work, much attention was given to the interaction behavior and its underlying mechanisms of the three frequently occurring processes in 316LN SS: DSA, creep and thermal recovery. Its influence on the cyclic deformation, failure mode and life behavior was elaborately discussed through creep-fatigue tests with different tensile hold periods based on transmission electron microscopy (TEM) characterization techniques.

2. Experiments

2.1 Material and Specimen

The chemical composition (in wt.%) of the 316LN SS used in this work is 0.018 C, 0.002 S, 0.22 Si, 0.11 N, 0.023 P, 1.42 Mn, 17.20 Cr, 12.95 Ni, 0.018 Co, 2.19 Mo, 0.033 Cu, 0.068 Nb, <0.01 Ti and balance Fe. The microstructure of the as-received material after solution heat treatment (1090 °C for 5.5 h), with an average grain size of approximately 229 μm determined by the EBSD characterization, is shown in

Fig. 1(a). The geometry of the specimen used in all creep-fatigue tests in this work is illustrated in Fig. 1(b).

2.2 Testing System and Experimental Details

Mechanical loads were applied by a computer-controlled hydraulic testing machine (MTS 370.02) with an axial force capacity of ± 25 kN. An induction heating generator with a power rate of 10 kW and an operating frequency of 15-35 kHz was employed for specimen heating. A K-type thermocouple with a diameter of 0.25 mm was spot-welded at the middle of the specimen gauge section to control and measure the temperature. A handmade induction coil was utilized to obtain a uniformly distributed temperature field within the specimen gauge section. Before each test, three K-type thermocouples were used to adjust the position and geometry of the induction coil. Then, only one thermocouple was utilized to reduce the damage caused by the thermocouple welding spot. The desired mechanical strain was applied to the specimen by a high-temperature extensometer (Epsilon 7650) with a gauge length of 12.5 mm. The LCF and creep-fatigue tests were performed at a constant strain amplitude of $\pm 0.8\%$ at 550 °C with various tensile hold periods: 0 s, 60 s, 120 s, 300 s, and 1800 s. The fully reversed total strain control mode with a strain rate of 0.02%/s was used. The failure criterion in this work was a 10% reduction in the maximum tensile stress, which generally corresponds to the formation of macroscopic cracks (Ref 30).

2.3 Microscopic Characterization

The fracture surface morphology was observed by scanning electron microscopy (SEM). Transmission electron microscopy (TEM) at a voltage of 300 kV was utilized to observe the dislocation microstructure. The samples used for TEM observations were sectioned parallel to the specimen axial direction, mechanically polished down to 50 μm, and electrochemically polished using an electrolyte of 10% perchloric acid in ethanol.

3. Results

3.1 Cyclic Stress Response

The effect of tensile hold periods on the cyclic stress response of 316LN SS is shown in Fig. 2. The cyclic stress response curve depicts the evolution of the stress amplitude versus the number of cycles. The loading condition expressed as '0 s' is the test without a hold period, i.e., a continuous LCF test. All tests show initial cyclic hardening followed by cyclic softening until the rapid stress drop associated with the formation of macrocracks occurs. The initial cyclic hardening is generally caused by the combined effect of DSA and the multiplication and mutual interaction of dislocations (Ref 21, 22). The different evolution behaviors of dislocations and DSA activity with various hold periods result in the difference in cyclic stress response behavior. A detailed explanation is provided in Sect. 4.1.

3.2 Deformation Mechanisms

3.2.1 Dynamic Strain Aging. Figure 3(a, b, c) shows the half-life cycle hysteresis loop with a hold period of 120 s and enlarged views of its tensile and compressive plastic regimes,
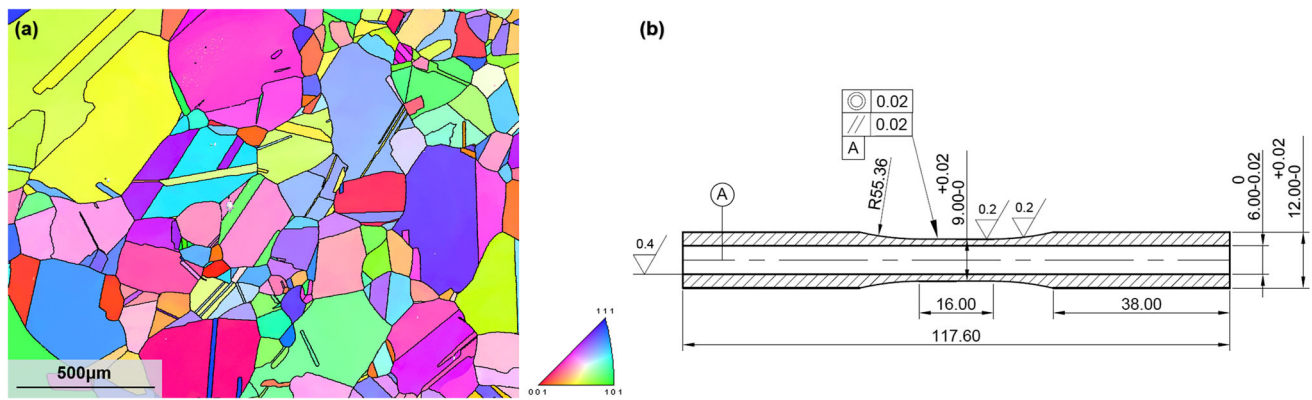
Fig. 1 (a) Microstructure of the as-received 316LN SS. (b) Geometry of the specimen (dimensions in mm)
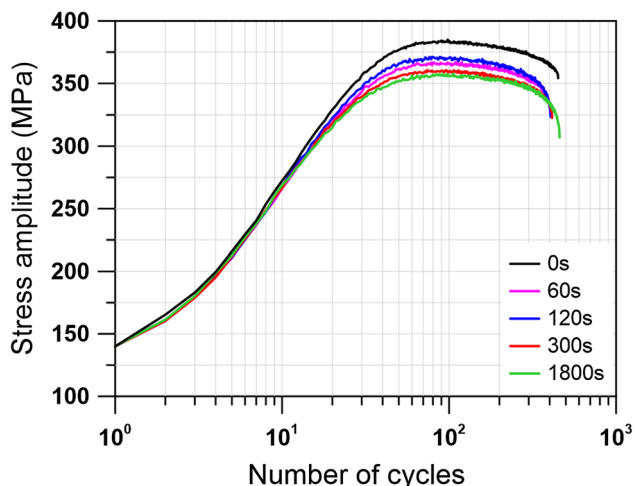

Fig. 2 Cyclic stress response in creep-fatigue tests with various hold periods

where the prominent stress serrations can be observed clearly, implying the occurrence of DSA. The definition of stress serration is demonstrated in Fig. 4(a). The number of serrations of every stress–strain hysteresis loop, an indication of the frequency of periodic dislocation pinning and unpinning processes, is used in this paper to quantitatively characterize the DSA intensity (Ref 31). The number of serrations is calculated by a MATLAB subroutine. Specifically, the stress values of three consecutive points (for example, points C, D and E in Fig. 4(b)) are compared, and the stress serration will be counted when the stress value of the middle point is less than the stress values of the two adjacent data points. As shown in Fig. 5(a), the number of serrations presents a marked dependence on the loading direction; specifically, more stress serrations are observed in the plastic strain regime of the compressive half-cycle than in that of the tensile half-cycle. A similar result was also reported in Ref 31, which was attributed to the difference in vacancy mobility affected by the hydrostatic stress (Ref 22, 31, 32). The new discovery in this work is that the number of stress serrations significantly decreases with increasing hold period, as shown in Fig. 5(a). Figure 5(b) presents the blown-up portion of the area marked in Fig. 5(a), showing the evolution behavior of serration numbers during the initial 100 cycles. The dashed vertical lines in Fig. 5(b) indicate

that the evolution of DSA reaches a stabilized stage. The number of stress serrations reaches a stable state more rapidly after the continuous reduction with the increase in hold period.

3.2.2 Stress Relaxation Behavior. The decrease in stress with increasing time during hold period is called stress relaxation. The relaxation of stress response is attributed to the dynamic thermal recovery inside crystals (Ref 33). Specifically, the recovery process during the hold period promotes the annihilation of dislocations, leading to the occurrence of stress relaxation, during which the creep deformation develops when the relaxation strain rate decreases to the critical value of 10^{-4} s^{-1} (Ref 2, 20). Correspondingly, part of the elastic component of the strain transforms to inelastic strain. The hold period exerts a significant influence on the evolution behavior of stress relaxation, as illustrated in Fig. 6, where a longer dwell time corresponds to a larger amount of stress relaxation. However, the opposite result was reported in Ref 9. Reddy et al. (Ref 9) attributed the decrease in the amount of stress relaxation with increasing hold period to the persistence of matrix hardening, which was caused by the promoted tendency to planar slip and enhanced strengthening effect due to the higher nitrogen content, 0.22 wt.%, compared to the lower nitrogen content of 0.11 wt.% in the present work. In addition, irrespective of the dwell time, the stress relaxation process includes two stages: the initial fast relaxation and subsequent stable relaxation stages, which is consistent with the conclusion provided by Sun et al. (Ref 34).

The inelastic relaxation strain rate $\dot{\varepsilon}_{in}$, defined in Eq 1 below, during the hold period of the half-life cycle is utilized to determine the proportion of creep damage (Ref 2, 20).

$$\dot{\varepsilon}_{in} = \frac{\dot{\sigma}}{E} = \frac{\Delta\sigma}{\Delta t} \cdot \frac{1}{E} \qquad (Eq\ 1)$$

where $\dot{\sigma}$ is the slope of the stress curve during the hold period and E is the Young's modulus acquired from the elastic phase in the stress–strain hysteresis loop of the half-life cycle. In order to determine the inelastic strain rate, which is defined in Eq 1 as the ratio of derivative of stress to elastic modulus, the stress value during the hold period needs to be calculated firstly based on the empirical formula proposed by Feltham (Ref 35), as shown in Eq 2.

$$\sigma = \sigma_0 - \sigma_0 \cdot B'' \ln(b \cdot t + 1) \qquad (Eq\ 2)$$
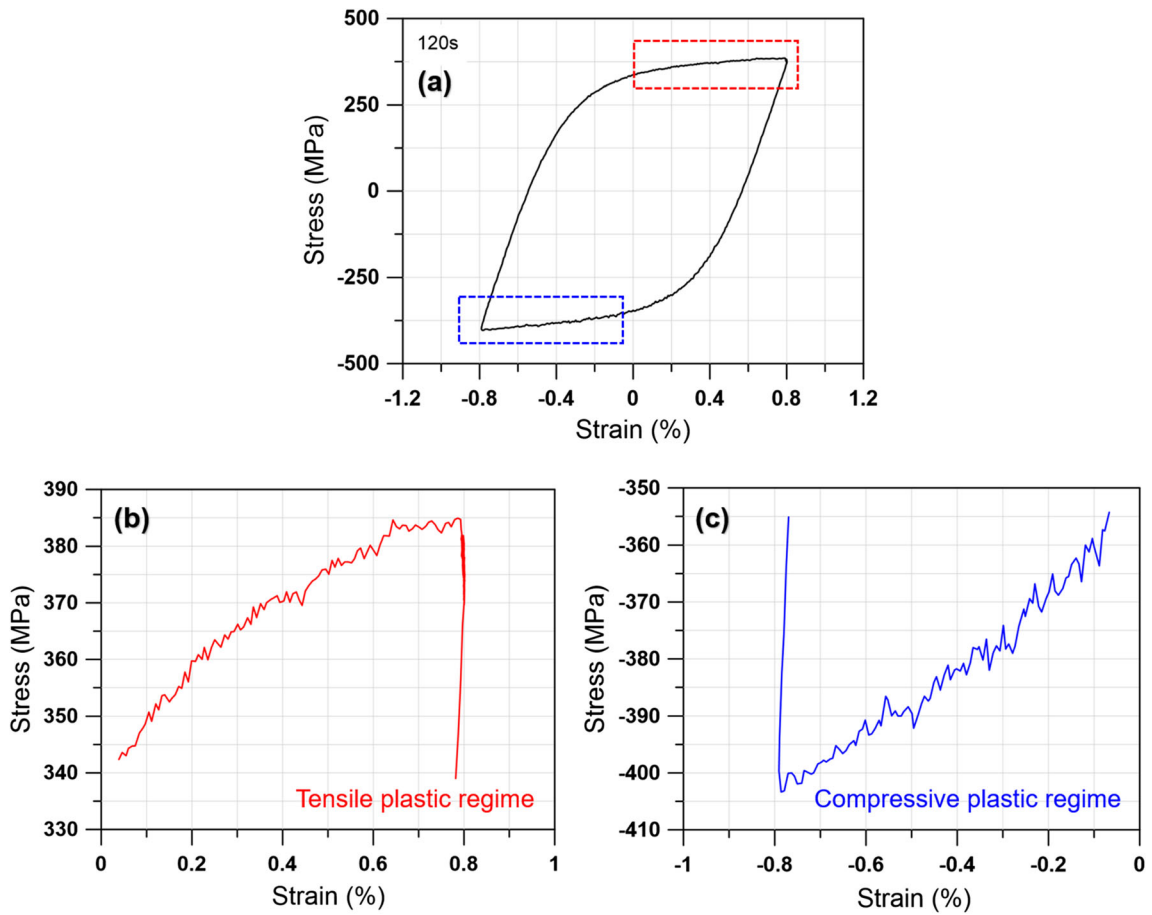
Fig. 3 (a) Half-life cycle hysteresis loop with a hold period of 120 s and enlarged views of the (b) tensile plastic regime and (c) compressive plastic regime.
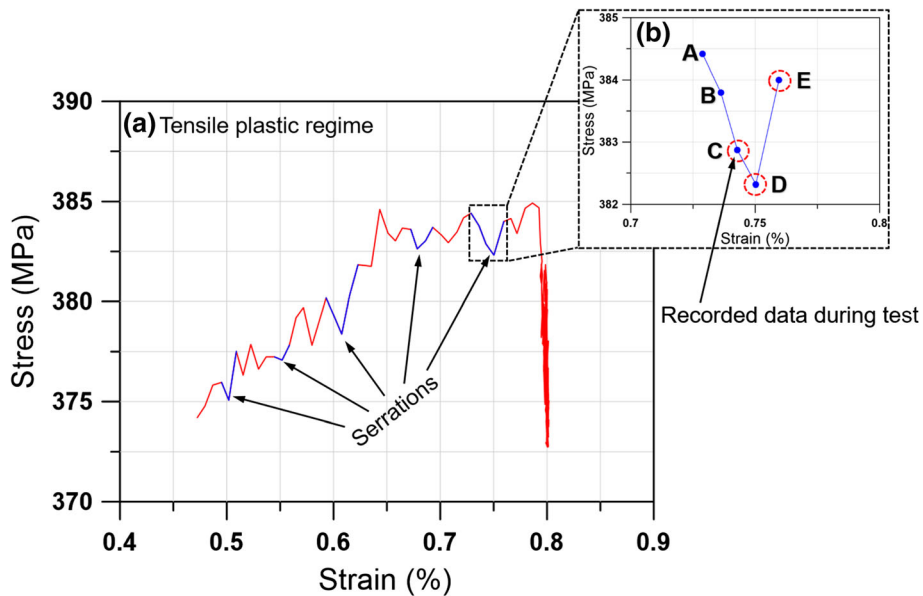

Fig. 4 (a) Tensile plastic regime of the half-life cycle hysteresis loop with a hold period of 120 s and (b) enlarged view of the region within the dashed lines in (a).
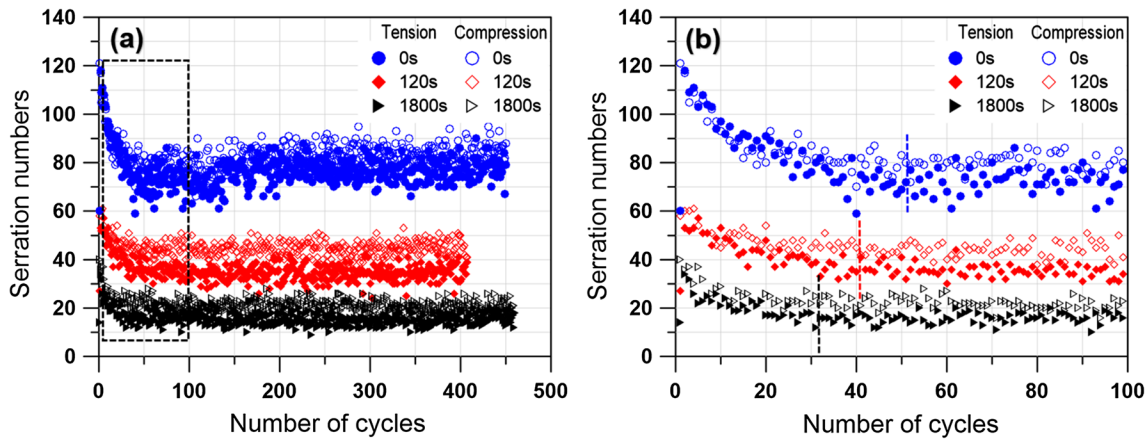
Fig. 5 (a) Variation in the stress serration numbers in tensile and compressive plastic deformation regions with various hold periods and (b) enlarged view of the region within the dashed lines in (a)
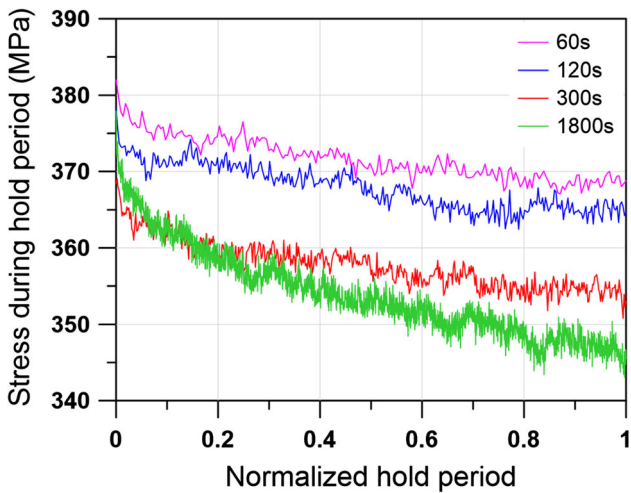

Fig. 6 Stress relaxation behavior during the hold period of the half-life cycle

Table 1 Values of the parameters in the empirical formula proposed by Feltham

	σ_0, MPa	B''	b
60 s	382	0.007929	1.28
120 s	378.11	0.008559	0.4806
300 s	368.42	0.009557	0.1696
1800 s	377.91	0.01756	0.05225

which means that no significant creep damage develops. Moreover, during the hold period of 300 s and 1800 s, the duration with inelastic strain rates less than 10^{-4} s^{-1} is 89.83 s and 1388.82 s, respectively. Therefore, it can be inferred that marked creep deformation occurs when the dwell time increases to 300 s and 1800 s, in which the time when the inelastic strain rate is less than 10^{-4} s^{-1} accounts for 30% and 77% of the whole hold period, respectively.

The stress relaxation behavior of creep-fatigue tests during the whole life and their fitting curves are shown in Fig. 8(a, b). The stress relaxation increases rapidly in the first few cycles, followed by a lower rate until the approximately stabilized state is reached. The stress relaxation in the whole life has a logarithmic relationship with the number of cycles and is consistent with the evolution behavior of the cyclic stress response, which implies that the stress response has a significant influence on the stress relaxation behavior. The result of fitting and the stress relaxation evolution of the first 20 cycles are shown in Fig. 8(b). The magnitude of stress relaxation increases with increasing hold period.

3.3 Fatigue Life

Generally, the fatigue life degrades when a hold period is introduced at the maximum tensile stress or strain for austenitic stainless steel, owing to the creep mechanism associated with stress relaxation (Ref 3, 18, 20, 21). However, there is no significant change in the fatigue lives during creep-fatigue tests with increasing hold period, as shown in Fig. 9(a). Interestingly,
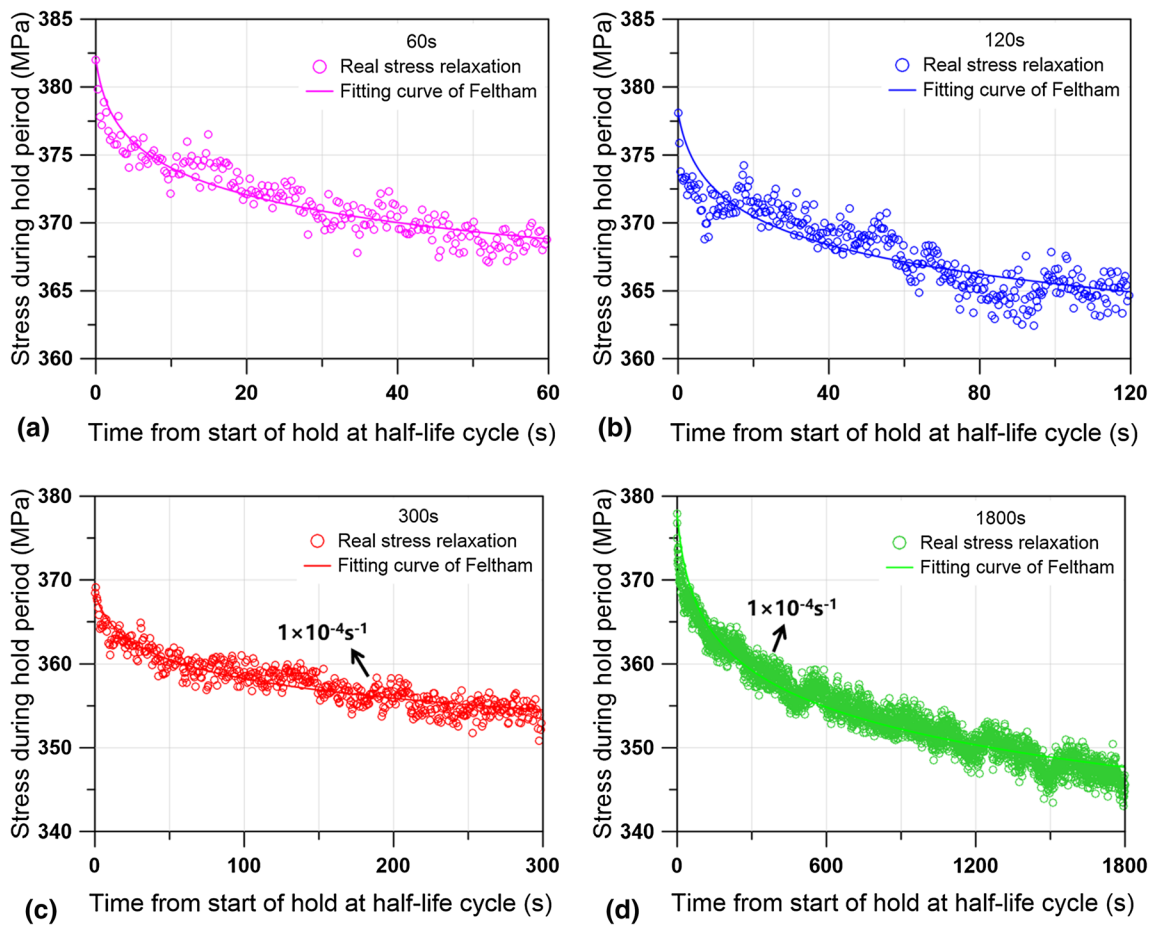
where σ_0 is the stress value at the start of the hold period, t is time, and b and B'' are coefficients. The detailed values of the parameters in Eq 2 are given in Table 1.

The stress relaxation behavior at the half-life cycle of creep-fatigue tests and their fitting curves (Ref 35) are shown in Fig. 7. The value of the inelastic strain rate, 10^{-4} s^{-1}, is the critical value for the occurrence of creep deformation (Ref 2, 20, 36). The point corresponding to the inelastic strain rate of 10^{-4} s^{-1} is marked in Fig. 7(c, d). The proportion of creep deformation is defined as the ratio of the duration with inelastic strain rates less than 10^{-4} s^{-1} to the total duration of the hold period in the half-life cycle. The minimum inelastic strain rate obtained during the process of stress relaxation and the proportion of the region with an inelastic strain rate lower than 10^{-4} s^{-1} during the whole hold period are provided in Table 2. Table 2 shows that the minimum values of the inelastic strain rate during the whole stress relaxation period in the tests with hold times of 60 s and 120 s are larger than 10^{-4} s^{-1},

Fig. 7 Stress relaxation and Feltham curve (Ref [35]) at the half-life cycle with hold periods of (a) 60 s, (b) 120 s, (c) 300 s, and (d) 1800 s

Table 2 Minimum inelastic strain rate and proportion of creep damage

	The minimum inelastic strain rate, s^{-1}	The proportion of inelastic strain rates less than 10^{-4} s^{-1}, %
60s	3.75×10^{-4}	0
120s	1.73×10^{-4}	0
300s	7.8×10^{-5}	30
1800s	1.4×10^{-5}	77

the fatigue life increases slightly to the level of the continuous low-cycle fatigue test when the hold period increases to 1800 s. A saturated state of fatigue life was achieved with increasing hold period in Ref. 12, 37, 38. Sauzay et al. (Ref 39) pointed out that this phenomenon was related to the decreased stress amplitude. However, Fig. 2 shows that the reduction in stress amplitude is not significant with increasing hold time, which is not the reason for the minimal variation in fatigue life in the present work. In addition, the time to failure calculated by the number of cycles multiplied by the time of each cycle is indicated in Fig. 9(b), demonstrating a linear increase with the hold time, although the fatigue lives are similar.

3.4 Fractographic Morphology

Figure 10, 11 and 12 demonstrate the fracture surface morphologies in creep-fatigue tests with dwell times of 60 s, 120 s and 1800 s, respectively. All the samples show the mixed cracking mode; specifically, crack initiation and early crack growth present an intergranular mode, while subsequent crack propagation takes place transgranularly. Crack initiation is dominated by oxidation (Ref 21), and the initial crack propagation is promoted by creep, followed by fatigue-dominated propagation and failure. Figure 10(b), 11(c) and 12(c) show that creep damage caused by the hold period leads to intergranular propagation and that the proportion of inter-
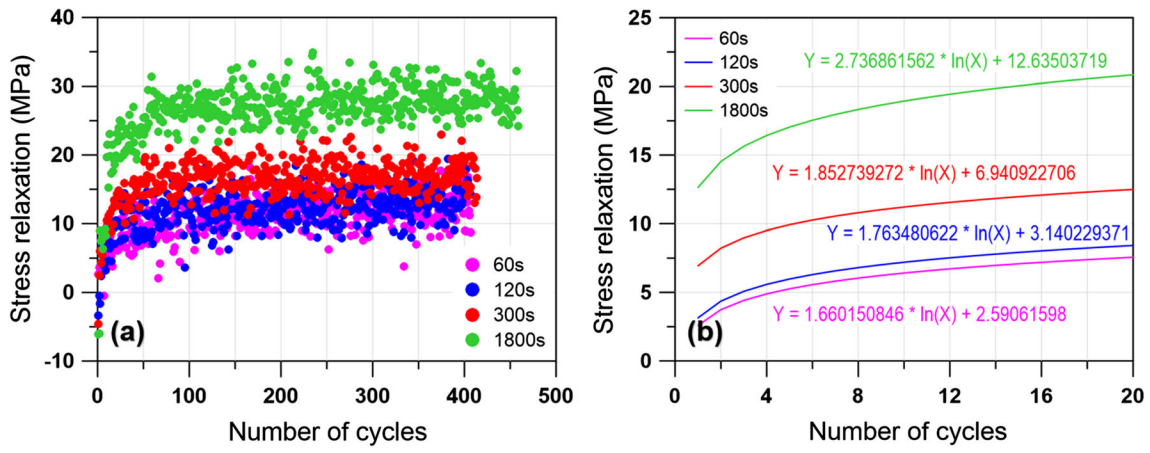
Fig. 8 (a) Stress relaxation behavior of creep-fatigue tests during the whole life. (b) Fitting curves of the stress relaxation behavior during the first 20 cycles
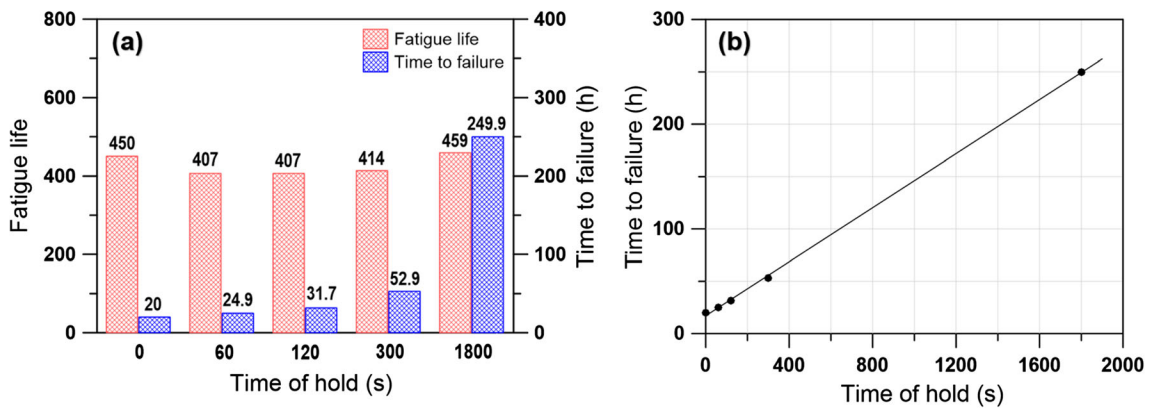

Fig. 9 (a) Fatigue life and time to failure in creep-fatigue tests with different hold periods and (b) linear relationship between the time to failure and hold period
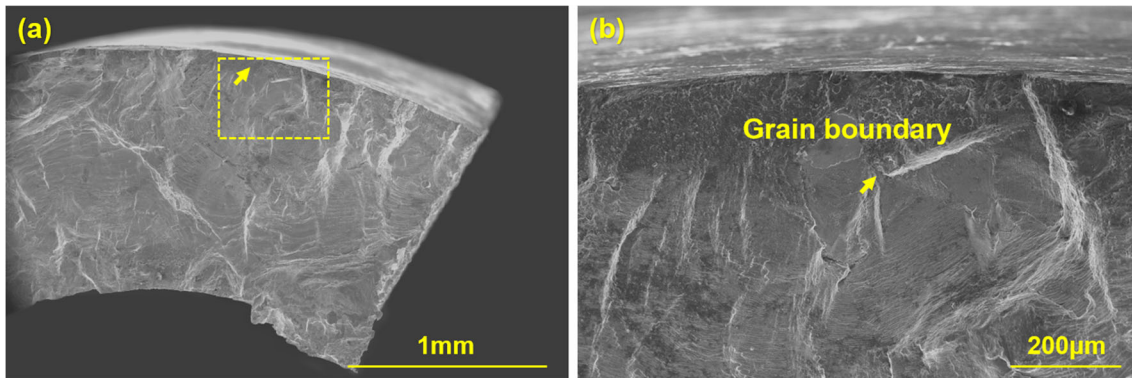

Fig. 10 (a) Fractographic morphology of the specimen with a hold period of 60 s and (b) enlarged view of the region within the dashed lines in (a)
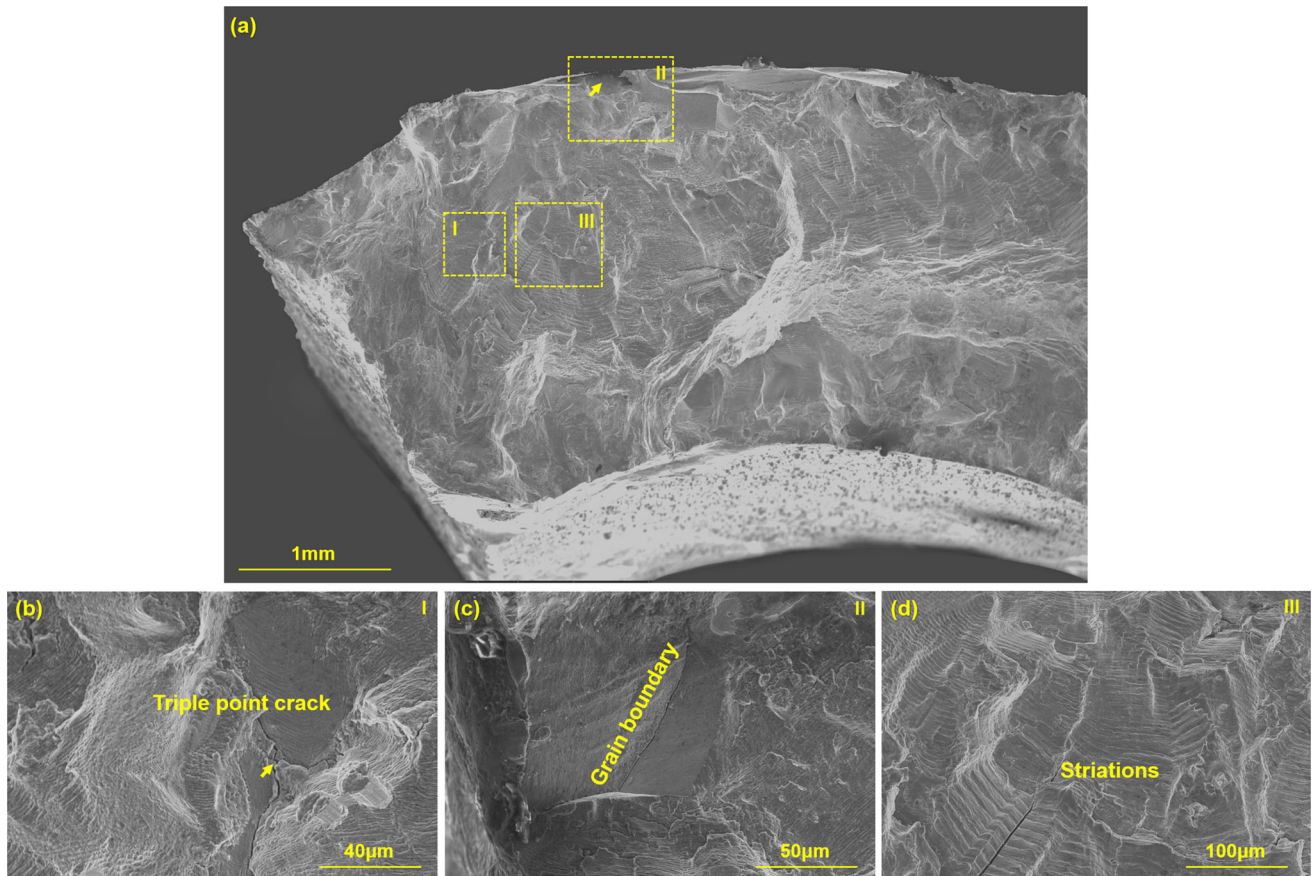
Fig. 11 (a) Fractographic morphology of the specimen with a hold period of 120 s and (b), (c), (d) enlarged views of regions within the dashed lines in (a)

granular cracks increases with increasing hold period. However, the appearance of substantial fatigue striations indicates that the fatigue damage is still strong, even when the hold period reaches 1800 s. This is probably because large-scale diffusional growth of cavities is not possible in polycrystals in a uniaxial state of stress (Ref 18).

3.5 Dislocation Microstructure Characterization

To understand the deformation mechanisms, TEM was utilized to analyze the dislocation substructure within the fractured specimens. Dislocation structures depend significantly on the hold period (Ref 9). Figure 13 shows the TEM characterization results of creep-fatigue tests with hold periods of 120 s, 300 s and 1800 s. The planar slip of dislocations characterized by the formation of well-defined planar slip bands and a high density of dislocation tangles, as shown in Fig. 13(a, b), accommodate plastic deformation. With the increase in the hold period, the transition in terms of the dislocation slip mode from planar slip to wavy slip occurs. The dislocation morphology presents a wall/channel structure in the test with a hold period of 300 s, as illustrated in Fig. 13(c, d). When the dwell time reaches 1800 s, the formation of well-defined elongated cells with a lower dislocation density within the cell interior is demonstrated in Fig. 13(e, f), which corresponds to a greater extent of recovery.

4. Discussion

4.1 Cyclic Hardening Analysis Based on DSA and Thermal Recovery

For 316LN SS, the initial cyclic hardening behavior is primarily attributed to the combined effects of dislocation-solute atom interactions and dislocation-dislocation interactions and is affected by the combined interactions between stress relaxation and DSA. During the process of cyclic hardening, the increased stress amplitude with an increasing number of cycles results in a higher tensile stress at the start of stress relaxation, which provides a larger driving force for dislocation motion during the recovery process, consequently resulting in an increase in the amount of stress relaxation, as shown in Fig. 8(a). However, on account of the enhanced cross-slip of screw dislocations, the pinning frequency of solid solute atoms is reduced, which leads to a decrease in DSA activity, as reflected by a considerable decrease in the number of serrations with an increase in the duration of the tensile hold period, as shown in Fig. 5(a). Variations in DSA activity and the extent of thermal recovery result in different stress responses. The low-cycle fatigue test without a hold period produces little recovery, as well as the strongest DSA activity, thus leading to the greatest effect of hardening and the highest stress response. In the tests with hold periods of 60 s and 120 s, the application of
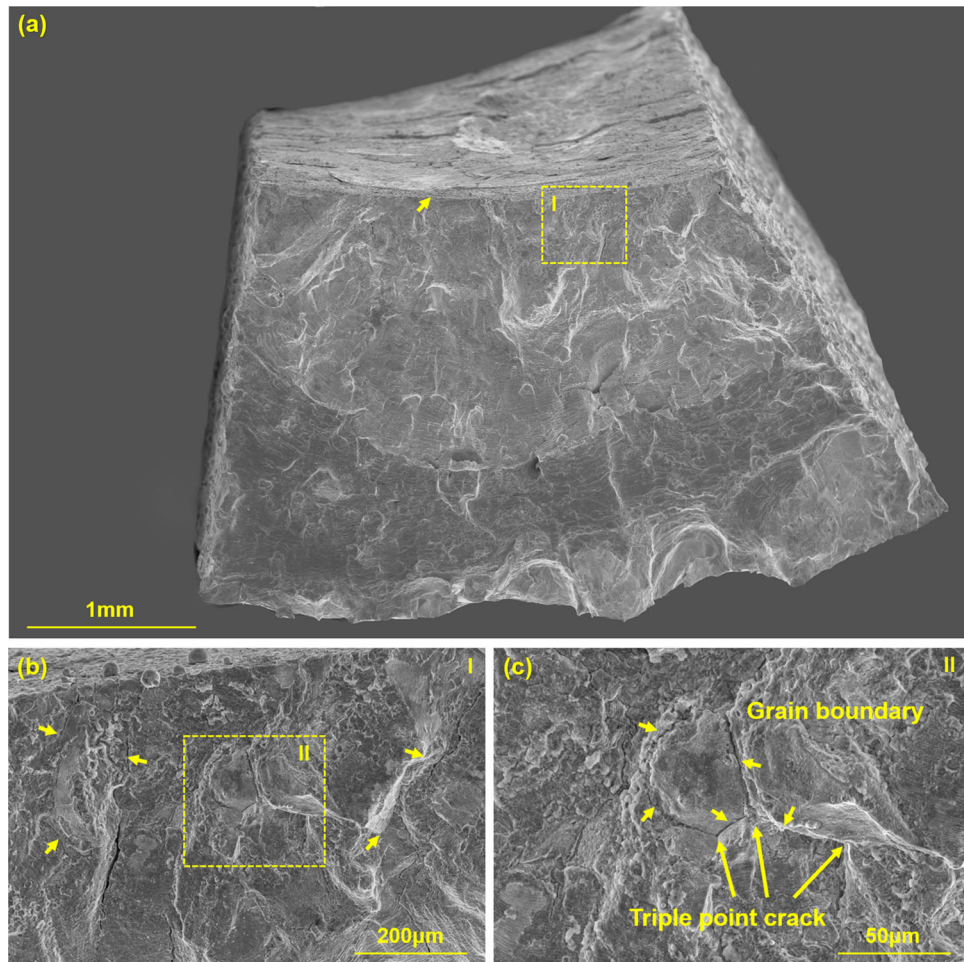
Fig. 12 (a) Fractographic morphology of the specimen with a hold period of 1800 s and (b), (c) enlarged views of regions within the dashed lines in (a), (b), respectively

a longer hold period tends to enhance the process of thermal recovery and decrease the DSA activity, which causes similar stress levels. With the hold period increasing to 300 s and 1800 s, the process of thermal recovery promotes the formation of dislocation walls/channels and elongated cells, in addition to the lower DSA activity, resulting in the lowest stress response.

4.2 Creep Damage Characterized by Inelastic Strain Rate

It is known that R-type creep cavities can form during tensile stress relaxation by the clustering of vacancies at the junctions between grain boundaries and second-phase particles under the influence of tensile stress (Ref 3, 40-42). As a result, a longer hold period can produce more vacancies and increase their activity, leading to the enhancement of creep damage, which provides more sites and time required for the formation of R-type cavities (Ref 43). As shown in Fig. 14 and 15(a), cavities are almost invisible along grain boundaries when the duration of the hold period is less than 300 s. As the hold period increases to 300 s, there are more cavities that connect to form intergranular cracks, as presented in Fig. 15(b, c, d). When the hold period increases to 1800 s, cavities are almost completely connected, developing deep intergranular cracks, as demonstrated in Fig. 16(a-d).

In general, the amount of stress relaxation is associated with the intergranular damage caused by creep deformation during the hold period. Therefore, the relaxed stress at the half-life cycle is used to characterize creep damage during the whole life (Ref 3, 20). However, Hales (Ref 36) proposed that the amount of intergranular damage was directly related to the accumulated inelastic strain during the hold period. In addition, a higher rate of inelastic strain accumulation does not impart any significant creep damage because of the insufficient diffusion of vacancies required for the growth of grain boundary cavities (Ref 15). Therefore, the inelastic strain rates associated with the rapid relaxation period correspond to precipitation-free matrix deformation, while those observed in the slow relaxation period (inelastic strain rate $< 10^{-4}$ s^{-1}) are typical of creep deformation (Ref 2, 20, 36). Therefore, the tests with a hold period less than 300 s do not induce significant creep damage, and with the increase in hold period, the proportion corresponding to creep deformation increases, reaching 1388.82 s when the hold period is 1800 s. The analysis of the inelastic strain rate is also consistent with the SEM observations of fracture and intergranular cavitation.

4.3 Interaction Between DSA and Stress Relaxation

Generally, austenitic stainless steels subjected to mechanical cycling at elevated temperatures tend to develop a well-defined cell structure. However, DSA promotes the planar-type dislocation distribution as a result of the interaction between mobile
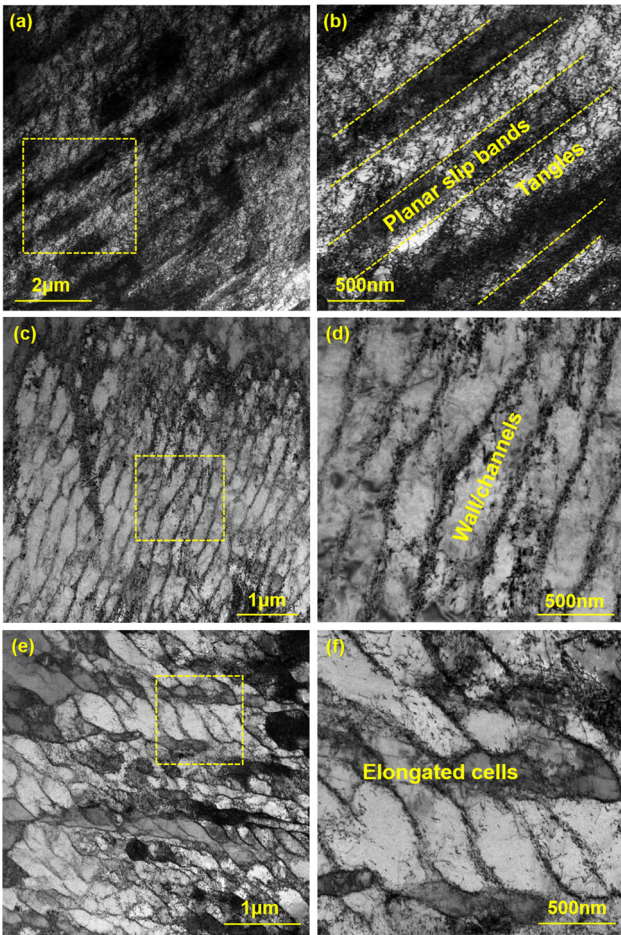
Fig. 13 Dislocation configurations of creep-fatigue tests with hold periods of (a) 120 s, (c) 300 s, (e) 1800 s and (b), (d), (f) enlarged views of the regions within the dashed lines in (a), (c), (e), respectively

dislocations and solute atmospheres (Ref 31, 44, 45). The diffusion of substitutional Cr atoms is responsible for the DSA behavior in the elevated temperature range because of their greater mobility (Ref 20, 31, 44). Compared with the LCF test at a constant temperature of 550 °C, creep-fatigue tests with the introduction of a hold period include another time-dependent effect, i.e., creep, which interacts with DSA. As a result, a longer hold period can produce more creep damage, promoting the development of dislocation cells through cross-slip, which reduces the pinning of solid solute atoms by changing the deformation mode from planar slip to cross-slip, as shown in Fig. 13. In addition, with the introduction of a hold period in every cycle, the process of dislocation rearrangement is enhanced, leading to the more rapid formation of the low-energy dislocation structure, as a result, the number of serrations stabilizes rapidly, as shown in Fig. 5(b). The evolution of DSA and stress relaxation presented in Fig. 17 shows a contrary trend during the initial stage. With the increasing number of cycles, the increased stress amplitude provides a larger driving force for dislocation motion during the recovery process, consequently resulting in an increase in the amount of stress relaxation. Meanwhile, the process of cross-slip is promoted, causing decreased DSA activity. The DSA activity and stress relaxation are basically stable when their interaction reaches a relative balance.

4.4 Analysis of Fatigue Life

The minimal variation in creep-fatigue life between the hold periods of 60 s, 120 s, and 300 s is attributed to the decreased DSA activity. DSA can induce a marked influence on the LCF behavior of stainless steels, such as promoting the planar slip of dislocations and strengthening the matrix, accelerating crack initiation and propagation and adversely affecting the cyclic life. With the introduction of a hold period in creep-fatigue tests, the combined effect of DSA and creep has a great influence on fatigue life. With the increase in the hold period,
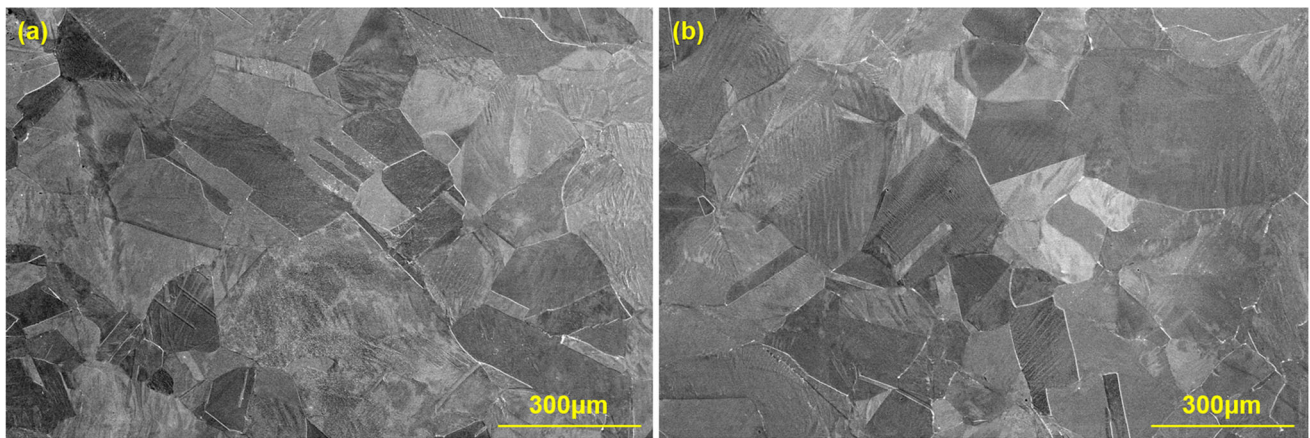

Fig. 14 Grain boundary morphology devoid of cavities with hold periods of (a) 0 s and (b) 60 s
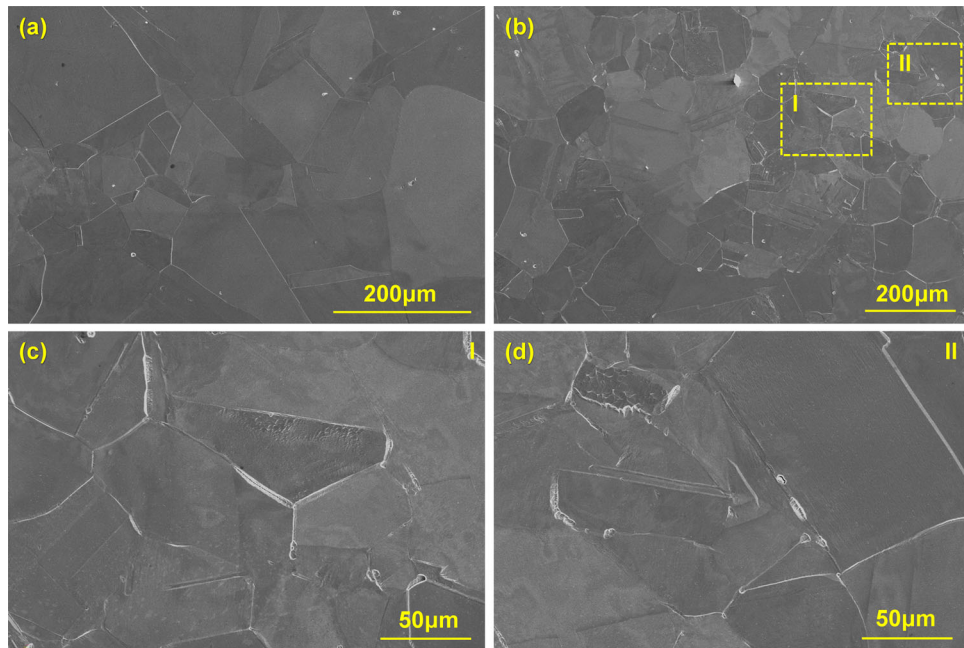
Fig. 15 (a) Grain boundary morphology devoid of cavities with a hold period of 120 s; (b) presence of intergranular cavities with a hold period of 300 s; and (c), (d) enlarged views of the regions within the dashed lines in (b)
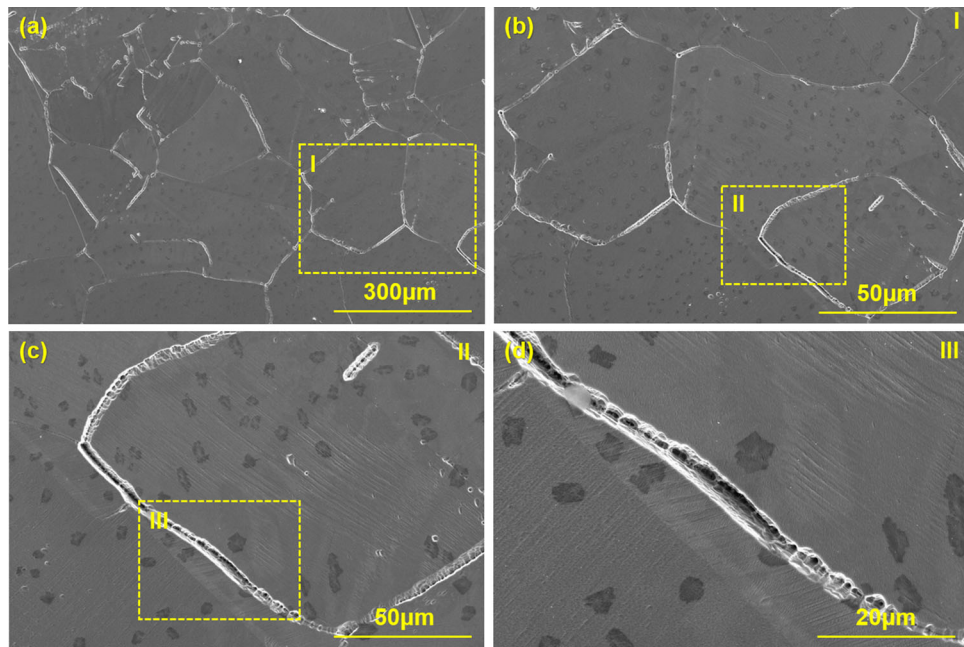

Fig. 16 (a) Intergranular cavitation with a hold period of 1800 s and (b), (c), (d) enlarged views of the regions within the dashed lines in (a), (b), (c), respectively

creep damage increases while DSA activity is reduced, which results in a marginal reduction in the fatigue life after the hold period is introduced, as shown in Fig. 9(a). However, when the hold period increases to 1800 s, the fatigue life is slightly increased due to the sufficient process of thermal recovery, as shown in Fig. 13(e, f). The recovery process has a significant effect on the cyclic deformation behavior of materials, which can influence the evolution of the dislocation structure and fatigue life (Ref 29). Thermal recovery promotes dislocation motion by the cross-slip of screw dislocations and climb of

edge dislocations and thereby increases the tendency toward the annihilation of dislocations, evolving into dislocations with low internal energy (Ref 46). Planar slip band impingements on grain boundaries during the process of DSA generate large internal stresses, which are believed to have a detrimental effect on the fatigue life. However, the recovery process reduces the frequency of planar slip, which results in a more uniform stress distribution within the grain interior, increasing the fatigue life slightly. Levaillant et al. (Ref 47) reported a slight recovery of fatigue life at a longer hold period, which was attributed to
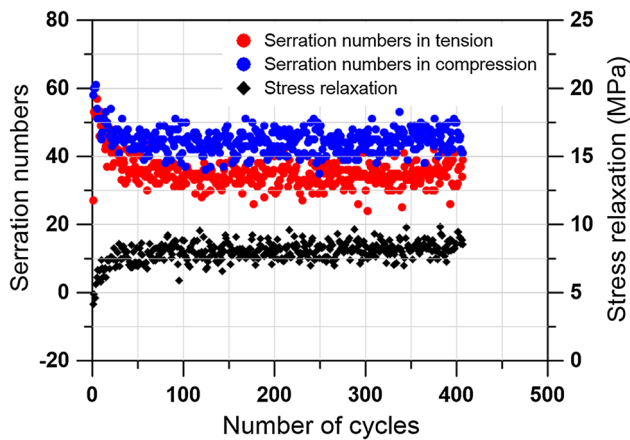
Fig. 17 Variation in stress relaxation and DSA in the test with a hold period of 120 s

thermal aging effects. Indeed, Brinkman and Korth (Ref 48) found that specimens subjected to aging treatment at 593 °C for 1000 h exhibited longer creep-fatigue lives than those without pretreatment. Wareing (Ref 37) attributed the longer fatigue life with the increase in hold period to the increase in cavity spacing along the grain boundary caused by thermal aging of the material, which was not observed in this present paper, possibly due to the absence of intergranular precipitation.

5. Conclusions

The cyclic deformation behavior and failure mechanism of 316LN stainless steel were studied by performing a series of creep-fatigue tests at 550 °C with various tensile hold periods at a constant strain amplitude. Several conclusions were drawn:

(1) The amount of creep damage was characterized by the inelastic strain rate. Creep damage only occurred when the hold period reached 300 s, and the proportion of creep damage increased with increasing hold period.
(2) Creep attenuated the pinning effect of solute atoms by changing the mode of deformation from planar slip to cross-slip; thus, the evolution trend of the amount of stress relaxation was in contrast with the evolution of the intensity of DSA with increasing hold period.
(3) The fatigue life remained approximately constant with the increase in hold period between 60 s and 300 s, which was ascribed to the decrease in DSA activity. However, the fatigue life increased slightly when the dwell time increased to 1800 s due to the increased thermal recovery process.

References

1. D.P.R. Palaparti, V. Ganesan, J. Christopher, and G.V.P. Reddy, Tensile Flow Analysis of Austenitic Type 316LN Stainless Steel: Effect of Nitrogen Content, *J. Mater. Eng. Perform.*, 2021, **30**(3), p 2074–2082
2. T.S. Kumar, A. Nagesha, and R. Kannan, Thermal Cycling Effects on the Creep-Fatigue Interaction in Type 316LN Austenitic Stainless Steel Weld Joint, *Int. J. Press. Vessels Pip.*, 2019, **178**, p 104009
3. P. Rodriguez and K.B.S. Rao, Nucleation and Growth of Cracks and Cavities under Creep-Fatigue Interaction, *Prog. Mater. Sci.*, 1993, **37**, p 403–480
4. S.C.S.P.K. Krovvidi, S. Goyal, and A.K. Bhaduri, Experimental and Numerical Investigation of High-Temperature Low-Cycle Fatigue and Creep-Fatigue Life of Bellows, *J. Mater. Eng. Perform.*, 2021, **30**(4), p 2742–2750
5. D. Ji, L.-C. Zhang, J. Ren, and D. Wang, Creep-Fatigue Interaction and Cyclic Strain Analysis in P92 Steel Based on Test, *J. Mater. Eng. Perform.*, 2015, **24**(4), p 1441–1451
6. D.W. Kim, J.-H. Chang, and W.-S. Ryu, Evaluation of the Creep–Fatigue Damage Mechanism of Type 316L and Type 316LN Stainless Steel, *Int. J. Press. Vessels Pip.*, 2008, **85**, p 378–384
7. X.-W. Wang, D.-G. Shang, and Z.-K. Guo, Multiaxial Creep-Fatigue Life Prediction under Variable Amplitude Loading at High Temperature, *J. Mater. Eng. Perform.*, 2019, **28**, p 1601–1611
8. Y.P. Yang and W.C. Mohr, Finite Element Creep-Fatigue Analysis of a Welded Furnace Roll for Identifying Failure Root Cause, *J. Mater. Eng. Perform.*, 2015, **24**(11), p 4388–4399
9. G.V.P. Reddy, R. Sandhya, S. Sankaran, P. Parameswaran, and K. Laha, Creep-Fatigue Interaction Behavior of 316LN Austenitic Stainless Steel with Varying Nitrogen Content, *Mater. Des.*, 2015, **88**, p 972–982
10. K. Kuwabara and A. Nitta, Thermal-Mechanical Low-Cycle Fatigue under Creep-Fatigue Interaction on Type 304 Stainless Steels, *Fatigue Eng. Mater. Struct.*, 1979, **2**, p 293–304
11. R. Koterazawa and T. Nosho, Creep-Fatigue Crack Growth and Fractography of Type 304 Stainless Steel at Elevated Temperature, *Fatigue Fract. Eng. Mater. Struct.*, 1991, **14**(1), p 1–9
12. X. Zhang, S.-T. Tu, and F. Xuan, Creep-Fatigue Endurance of 304 Stainless Steels, *Theor. Appl. Fract. Mech.*, 2014, **71**, p 51–66
13. D.S. Wood and P. Banks, The Creep/Fatigue Behaviour of Type 316 Steel under Reverse Bending Conditions, *Fatigue Fract. Eng. Mater. Struct.*, 1990, **13**(6), p 551–561
14. D.W. Kim, Influence of Nitrogen-Induced Grain Refinement on Mechanical Properties of Nitrogen Alloyed Type 316LN Stainless Steel, *J. Nucl. Mater.*, 2012, **420**, p 473–478
15. Y. Takahashi, H. Shibamoto, and K. Inoue, Study on Creep-Fatigue Life Prediction Methods for Low-Carbon Nitrogen-Controlled 316 Stainless Steel (316FR), *Nucl. Eng. Des.*, 2008, **238**, p 322–335
16. V. Ganesan, K. Laha, and M.D. Mathew, Influence of Nitrogen Content on the Evolution of Creep Damage in 316LN Stainless Steel, *Procedia Eng.*, 2014, **86**, p 58–65
17. R.P. Skelton and D. Gandy, Creep-Fatigue Damage Accumulation and Interaction Diagram Based on Metallographic Interpretation of Mechanisms, *Mater. High Temp.*, 2008, **25**(1), p 27–54
18. B.K. Min and R. Raj, Hold-Time Effects in High Temperature Fatigue, *Acta Metall.*, 1978, **26**, p 1007–1022
19. F. Benjamin, S. Maxime, C. Christel, N. Michel, and R. Véronique, High Temperature Creep-Fatigue-Oxidation Interactions in 9–12%Cr Martensitic Steels, *J. Nucl. Mater.*, 2009, **386–388**, p 418–421
20. V.S. Srinivasan, A. Nagesha, M. Valsan, K.B.S. Rao, S.L. Mannan, and D.H. Sastry, Effect of Hold-Time on Low Cycle Fatigue Behaviour of Nitrogen Bearing 316L Stainless Steel, *Int. J. Press. Vessels Pip.*, 1999, **76**, p 863–870
21. B. Li, Y. Zheng, S. Shi, Z. Zhang, and X. Chen, Cyclic Deformation and Cracking Behavior of 316LN Stainless Steel under Thermomechanical and Isothermal Fatigue Loadings, *Mater. Sci. Eng. A*, 2020, **773**, p 138866
22. M.S. Pham and S.R. Holdsworth, Dynamic Strain Ageing of AISI 316L during Cyclic Loading at 300 °C: Mechanism, Evolution, and its Effects, *Mater. Sci. Eng. A*, 2012, **556**, p 122–133

23. K.G. Samuel, S.L. Mannan, and P. Rodriguez, Serrated Yielding in AISI 316 Stainless Steel, *Acta Metall.*, 1988, **36**(8), p 2323–2327

24. D.W. Kim, W.G. Kim, and W.-S. Ryu, Role of Dynamic Strain Aging on Low Cycle Fatigue and Crack Propagation of Type 316L(N) Stainless Steel, *Int. J. Fatigue*, 2003, **25**, p 1203–1207

25. S.-G. Hong and S.-B. Lee, Mechanism of Dynamic Strain Aging and Characterization of its Effect on the Low-Cycle Fatigue Behavior in Type 316L Stainless Steel, *J. Nucl. Mater.*, 2005, **340**, p 307–314

26. L. Xu, F. Bao, L. Zhao, Y. Han, H. Jing, H. Yu, and X. Gong, Characterizing Microstructural Evolution and Low Cycle Fatigue Behavior of 316H Austenitic Steel at High-Temperatures, *J. Nucl. Mater.*, 2021, **546**, p 152758

27. S.J. Majumdar, Relationship of Creep, Creep-Fatigue, and Cavitation Damage in Type 304 Austenitic Stainless Steel, *Eng. Mater. Technol.*, 1989, **111**(2), p 123–131

28. M.L.G. Byrnes, M. Grujicic, and W.S. Owen, Nitrogen Strengthening of a Stable Austenitic Stainless Steel, *Acta Metall.*, 1987, **35**(7), p 1853–1862

29. G.V.P. Reddy, R. Kannan, K. Mariappan, R. Sandhya, S. Sankaran, and K.B.S. Rao, Effect of Strain Rate on Low Cycle Fatigue of 316LN Stainless Steel with Varying Nitrogen Content: Part-I Cyclic Deformation Behavior, *Int. J. Fatigue*, 2015, **81**, p 299–308

30. EUR 22281 EN, Validated code-of-practice for strain-controlled thermomechanical fatigue testing

31. B. Li, Y. Zheng, J. Zhao, S. Shi, Z. Zhang, and X. Chen, Cyclic Deformation Behavior and Dynamic Strain Aging of 316LN Stainless Steel under Low Cycle Fatigue Loadings at 550 °C, *Mater. Sci. Eng. A*, 2021, **818**, p 141411

32. B.K. Choudhary, Activation Energy for Serrated Flow in Type 316L(N) Austenitic Stainless Steel, *Mater. Sci. Eng. A*, 2014, **603**, p 160–168

33. R.T. Dewa, J.H. Park, S.J. Kim, and S.Y. Lee, High-Temperature Creep-Fatigue Behavior of Alloy 617, *Metals*, 2018, **8**, p 103

34. L. Sun, X.-G. Bao, S.-J. Guo, R.-Z. Wang, X.-C. Zhang, and S.-T. Tu, The Creep-Fatigue Behavior of a Nickel-Based Superalloy: Experiments Study and Cyclic Plastic Analysis, *Int. J. Fatigue*, 2021, **147**, p 106187

35. P. Feltham, Creep and Stress Relaxation in Alpha-Brass at Low Temperatures, *Philos. Mag.*, 1961, **6**(62), p 259

36. R. Hales, A Quantitative Metallographic Assessment of Structural Degradation of Type 316 Stainless Steel during Creep-Fatigue, *Fatigue Fract. Eng. Mater. Struct.*, 1980, **3**(4), p 339–356

37. J. Wareing, Creep-Fatigue Behaviour of Four Casts of Type 316 Stainless Steel, *Fatigue Fract. Eng. Mater. Struct.*, 1981, **4**(2), p 131–145

38. X. Wang, W. Zhang, J. Gong, and M.A. Wahab, Low Cycle Fatigue and Creep Fatigue Interaction Behavior of 9Cr-0.5Mo-1.8W-V-Nb Heat-Resistant Steel at High Temperature, *J. Nucl. Mater.*, 2018, **505**, p 73–84

39. M. Sauzay, M. Mottot, L. Allais, M. Noblecourt, I. Monnet, and J. Périnet, Creep-Fatigue Behaviour of an AISI Stainless Steel at 550 °C, *Nucl. Eng. Des.*, 2004, **232**, p 219–236

40. Z. Zhang, J. Tan, X. Wu, E.-H. Han, W. Ke, and J. Rao, Corrosion Fatigue Behavior and Crack-Tip Characteristic of 316LN Stainless Steel in High-Temperature Pressurized Water, *J. Nucl. Mater.*, 2019, **518**, p 21–29

41. H.C. Wu, B. Yang, S.L. Wang, and M.X. Zhang, Effect of Oxidation Behavior on the Corrosion Fatigue Crack Initiation and Propagation of 316LN Austenitic Stainless Steel in High Temperature Water, *Mater. Sci. Eng. A*, 2015, **633**, p 176–183

42. K.-H. Bae, H.-H. Kim, and S.-B. Lee, Competing Damage Mechanisms in the Thermo-Mechanical Fatigue of AISI 304L Stainless Steel, *Mater. Sci. Eng. A*, 2011, **529**, p 417–424

43. K.S. Min and S.W. Nam, Correlation Between Characteristics of Grain Boundary Carbides and Creep-Fatigue Properties in AISI 321 Stainless Steel, *J. Nucl. Mater.*, 2003, **322**, p 91–97

44. A. Nagesha, R. Kannan, P. Parameswaran, R. Sandhya, K.B.S. Rao, and V. Singh, A Comparative Study of Isothermal and Thermomechanical Fatigue on Type 316L(N) Austenitic Stainless Steel, *Mater. Sci. Eng. A*, 2010, **527**, p 5969–5975

45. C.Y. Jeong, S.W. Nam, and J. Ginsztler, Stress Dependence on Stress Relaxation Creep Rate during Tensile Holding under Creep-Fatigue Interaction in 1Cr-Mo-V Steel, *J. Mater. Sci.*, 1999, **34**, p 2513–2517

46. B. Li, Y. Zheng, S. Shi, Y. Liu, Y. Li, and X. Chen, Microcrack Initiation Mechanisms of 316LN Austenitic Stainless Steel under In-Phase Thermomechanical Fatigue Loading, *Mater. Sci. Eng. A*, 2019, **752**, p 1–14

47. C. Levaillant, J. Grattier, M. Mottot, and A. Pineau, Creep and Creep-Fatigue Intergranular Damage in Austenitic Stainless Steels: Discussion of the Creep-Dominated Regime, *J. ASTM Int.*, 1988, **942**, p 414–437

48. C.R. Brinkman and G.E. Korth, Heat-to-Heat Variations in the Fatigue and Creep-Fatigue Behavior of AISI Type 304 Stainless Steel at 593 °C, *J. Nucl. Mater.*, 1973, **48**, p 293–306